Communication

Nanoscale Metal-Organic Frameworks for Ratiometric Oxygen Sensing in Live Cells

Ruoyu Xu, Youfu Wang, Xiaopin Duan, Kuangda Lu, Daniel Micheroni, Aiguo Hu, and Wenbin Lin

J. Am. Chem. Soc., **Just Accepted Manuscript** • DOI: 10.1021/jacs.5b13458 • Publication Date (Web): 11 Feb 2016

Nanoscale Metal-Organic Frameworks for Ratiometric Oxygen Sensing in Live Cells

Ruoyu Xu,[†,1] Youfu Wang,[†,1,2] Xiaopin Duan,[1] Kuangda Lu,[1] Daniel Micheroni,[1] Aiguo Hu,[2] and Wenbin Lin,*[,1]

[1]Department of Chemistry, University of Chicago, 929 E 57th St, Chicago, Illinois 60637, United States

[2]Shanghai Key Laboratory of Advanced Polymeric Materials, School of Materials Science and Engineering, East China University of Science and Technology, Shanghai 200237, China

Supporting Information Placeholder

ABSTRACT: We report the design of a phosphorescence/fluorescence dual-emissive nanoscale metal organic framework (NMOF), R-UiO, as an intracellular oxygen (O_2) sensor. R-UiO contains a Pt(II)-porphyrin ligand as an O_2-sensitive probe and a Rhodamine-B isothiocyanate (RITC) ligand as an O_2-insensitive reference probe, and exhibits good crystallinity, high stability, and excellent ratiometric luminescence response to O_2 partial pressure. *In vitro* experiments confirmed the applicability of R-UiO as an intracellular O_2 biosensor. This work is the first report of a NMOF-based intracellular oxygen sensor and should inspire the design of ratiometric NMOF sensors for other important analytes in biological systems.

Oxygen (O_2) is a vital component in aerobic respiration that provides metabolic energy to cells. Hypoxia — a reduction in normal levels of O_2— is related to various diseases,[1] including vascular disease, pulmonary disease, and cancer.[2] For instance, sustained hypoxia in a growing tumor can result in a more aggressive phenotype.[3] Monitoring and quantifying O_2 levels in living cells are thus of great importance for cancer diagnosis, tumor pathophysiology assessment, and the evaluation of the therapeutic effects of anticancer treatments. O_2 tension can be detected and measured by several methods, including polarographic O_2 needle electrodes,[4] immunohistochemical staining,[5] positron emission tomography imaging,[6] magnetic resonance imaging[7] and photoluminescence imaging.[8] Because of their high sensitivity and outstanding spatial resolution, photoluminescence-based techniques provide particularly powerful tools for sensing O_2 in living cells. Ratiometric sensing, which uses an O_2-insensitive reference and an O_2-sensitive probe to measure emission ratios at two different wavelengths, can compensate for signal changes caused by disturbance from external environment, such as light scattering and fluctuations in the excitation source,[9] allowing for accurate measurements of O_2 concentrations. Since Kopelman and co-workers first developed PEEBLEs (probes encapsulated by biologically localized embedding) containing a cyanine-dye standard and a Pt-porphyrin phosphor for ratiometric O_2 sensing,[10] a number of polymeric nanoparticles,[8c, 8e] silica gels,[11] and quantum dots[12] have emerged as promising ratiometric O_2 sensors.

Metal-organic frameworks (MOFs) are an emerging class of porous materials built from metal ions or clusters bridged by organic linkers that have been explored as chemical sensors.[13] Nanoscale MOFs (NMOFs) have also been used for small molecule sensing[14] and biomedical imaging.[15] NMOFs exhibit several characteristics that make them ideal nanomaterials for biological and biomedical applications. First, NMOFs have good crystallinity and structural tunability, which allow synthetic elaborations for specific applications. Second, NMOFs are highly porous, which allows them to accommodate high loadings of imaging/therapeutic agents, quickly diffuse small molecules (i.e., drugs, analysts), and prevent dye self-quenching. Third, NMOFs do not suffer from agent leaching due to covalent bonding. Fourth, NMOFs are intrinsically biodegradable in the long term due to their relatively labile metal–ligand bonds.[16] For example, we have recently used a fluorescent NMOF for real-time intracellular pH sensing[15a] and a porphyrin-based NMOF in photodynamic therapy.[17] Herein, we report the first NMOF probe for ratiometric O_2 sensing in live cells.

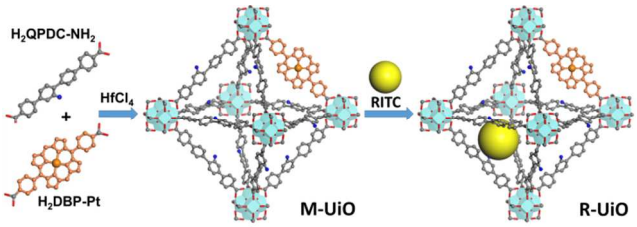

Scheme 1. Synthesis of mixed-ligand M-UiO NMOF and its postsynthesis modification to afford R-UiO NMOF.

We hypothesized that an NMOF with both O_2-independent and –sensitive ligands would serve as an excellent ratiometric O_2 sensor by taking advantage of the aforementioned features of NMOFs. Pt-5, 15-di(*p*-benzoato)-porphyrin (DBP-Pt) was chosen as an O_2-sensitive bridging ligand whereas Rhodamine-B isothiocyanate (RITC) conjugated quaterphenyldicarboxylate (QPDC) was used as an O_2-independent ligand to construct a ratiometric NMOF, R-UiO (Scheme 1). Pt-porphyrin shows bright phosphorescence with a long-lived triplet state at ambient temperature, and its phosphorescence intensity is highly dependent on O_2 concentration, making it an ideal choice as an O_2-sensitive probe in ratiometric O_2 sensing.[8c-e,10] We selected Rhodamine-B as

a reference dye for the following reasons: (1) Absorption of Rhodamine-B and H_2DBP-Pt at 500-540 nm allows for the simultaneous excitation of both dyes (Figure S5); (2) The non-overlap of Rhodamine-B fluorescence (570 nm) and H_2DBP-Pt phosphorescence (630 nm) (Figure S5) facilitates ratiometric luminescence quantifications; (3) The pH-independent fluorescence of Rhodamine-B at pH > 6 prevents disturbance due to cellular pH changes;[18] (4) Emissions of both dyes at relatively long wavelengths (> 570 nm) minimize background autofluorescence from live cells.

We further hypothesized that a mixed ligand NMOF with both DBP-Pt and amino-quaterphenyldicarboxylate (QPDC-NH_2) could be built due to the similar lengths of these ligands. We observed that the unit cell parameter of Zn-DPDBP-UiO[17] (38.76 Å, DPDBP: 10, 20-diphenyl-5, 15-di(*p*-benzoato)porphyrin), whose ligand is similar in structure to DBP-Pt, is only 0.2% larger than that of TPHN-UiO[19] (38.68 Å, TPHN: 4,4′-bis(carboxyphenyl)-2-nitro-1,1′-biphenyl). The QPDC-NH_2 ligands in the mixed ligand NMOF could be readily conjugated with RITC to afford the dual-emissive R-UiO NMOF. Furthermore, the relative intensities of RITC fluorescence and DBP-Pt phosphorescence can be tuned by adjusting the feed ratio of the two dyes during MOF synthesis and post-synthesis modification, respectively.

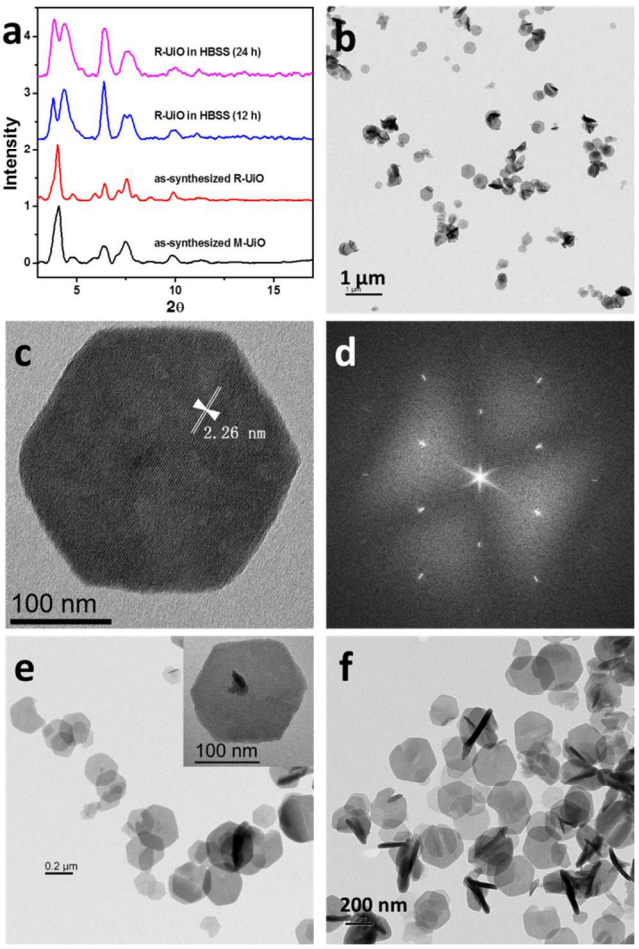

Figure 1. Structure and morphology of mixed ligand M-UiO and R-UiO NMOF. (a) PXRD patterns of M-UiO, as-synthesized R-UiO and R-UiO after incubation in HBSS for 12 h and 24 h. (b) TEM, (c) high-resolution TEM and (d) fast Fourier transform patterns of M-UiO. TEM images of R-UiO (e) before and (f) after incubation in HBSS for 24 h.

H_2QPDC-NH_2 was obtained by Suzuki coupling between 4,4'-dibromo-2-amino-1,1'-biphenyl and 4-methoxycarbonyl-phenylboronic acid, followed by hydrolysis. H_2DBP-Pt was synthesized by metalation of 5,15-di(4-methoxycarbonyl)porphyrin (Me_2DBP) with K_2PtCl_4 in benzonitrile under reflux, followed by hydrolysis in basic conditions, and characterized by NMR spectroscopy and mass spectrometry (Scheme S2). A solvothermal reaction between H_2DBP-Pt, H_2QPDC-NH_2 and $HfCl_4$ in N, N-dimethylformamide (DMF) at 80 °C afforded the mixed-ligand NMOF, M-UiO, as an orange powder (Scheme 1). Transmission electron microscopy (TEM) revealed hexagonal plate morphology with a diameter of ~200 nm and a thickness of ~30 nm (Figure 1b). Powder X-ray diffraction (PXRD), high-resolution TEM, and fast Fourier transform patterns showed that M-UiO displayed good crystallinity (Figures 1). The distance between adjacent secondary building units (SBUs) was measured to be ~2.26 nm by TEM, consistent with the distance of 2.18 nm calculated from the PXRD data. UV-vis spectrum of M-UiO showed only two Q-band peaks, suggesting no Pt leaching during NMOF synthesis (Figure S4).[19] Inductively coupled plasma–mass spectrometry (ICP-MS) gave a DBP-Pt: QPDC-NH2 molar ratio of 6.2:93.8 in M-UiO.

Rhodamine-B was covalently attached to M-UiO by forming the thiourea linkage between QPDC-NH_2 and RITC in R-UiO, which was confirmed by mass spectrometry (Figure S6). TEM images and PXRD patterns showed that R-UiO retained the plate-like morphology and the crystallinity of M-UiO (Figure 1a, 1f). Dynamic light scattering (DLS) measurements gave an average diameter of 177.8 (PDI = 0.064) and 181.1 (PDI = 0.079) for M-UiO and R-UiO, respectively. The loadings of Rhodamine-B could be adjusted by controlling the feed amount of RITC, leading to R-UiO-1 and R-UiO-2 that contain 0.6 mol% and 1.6 mol% Rhodamine-B, respectively (Figure S12 and S13).

R-UiO was incubated in Hank's Balanced Salt Solution (HBSS) buffer for 24 h to evaluate its stability in physiological conditions. After incubation, the d_{111} peak in the PXRD pattern was split into two peaks (Figure 1a), likely due to minor lattice distortion in the buffer solution. Nevertheless, TEM image clearly indicated the preservation of lattice fringes (Figure 2f, S9 and S10). Moreover, there is no Rhodamine-B or DBP-Pt leaching after incubation (Figure S8), suggesting adequate stability for oxygen sensing in the media.

To achieve ratiometric quantification using a single excitation and simultaneous detection of RITC fluorescence and DBP-Pt phosphorescence, there cannot be energy transfer from DBP-Pt to Rhodamine-B. This lack of energy transfer was confirmed by 1) a negligible overlap between H_2DBP-Pt emission and Rhodamine-B absorption (Figure S5), 2) the presence of only characteristic DBP-Pt phosphorescence, but not RITC fluorescence upon exciting R-UiO at 391 nm (corresponding to H_2DBP-Pt soret band, Figure S11) and 3) similar phosphorescence lifetimes of R-UiO and H_2DBP-Pt (Figure S16). Ratiometric sensing was first carried out by fluorimetry with a 514 nm excitation light source in order to match the laser in confocal laser scanning microscopy (CLSM). Under nitrogen-saturated atmosphere (pO_2 = 0 mmHg), R-UiO-1 showed a strong emission at 630 nm from DBP-Pt and a weak

emission at 570 nm attributed to RITC (Figure 2a). As pO_2 gradually increased to aerated atmosphere (pO_2 = 160 mmHg), the RITC fluorescence remained unchanged, while the DBP-Pt phosphorescence decreased significantly as expected. We quantitatively analyzed oxygen quenching by fitting the data to the Stern-Volmer equation,[20]

$$\frac{R_I^0}{R_I} = 1 + K_{SV} p_{O_2} \quad (1)$$

where K_{SV} is the Stern-Volmer constant, and $R_I^o = I_P^o/I_F^o$ and $R_I = I_P/I_F$ are the ratio of phosphorescence intensity to fluorescence intensity in the absence and presence of oxygen, respectively. R_I^o/R_I showed a good linear relationship with respect to pO_2 up to 80 mmHg (Figure 2b). Beyond this point, the ratio deviated from the Stern-Volmer plot (Figure S14). Such a deviation was also observed in previous reports[7, 21] and is probably related to the complicated dynamics involved in the MOF structure. Fortunately, pO_2 in biological tissues is typically below 70 mmHg (except in arterial blood).[22] Within this range, the intensity ratio fitted well to the Stern-Volmer equation with K_{SV} = 0.015 $mmHg^{-1}$. The O_2 quenching experiment proved that R-UiO is a good O2 sensor by providing pO_2-specific I_P/I_F ratios.

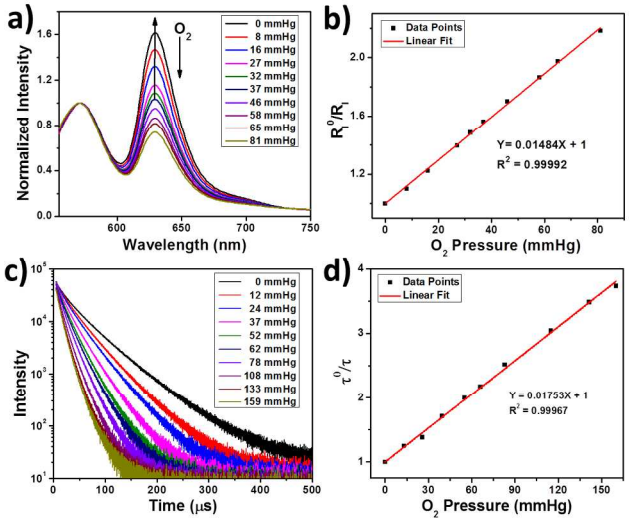

Figure 2. (a) Emission spectra (λ_{ex} = 514 nm) and (c) phosphorescent decays (λ_{ex} = 405 nm) of R-UiO-1 in HBSS buffer under various oxygen partial pressures. Plots of R_I^o/R_I (b) and τ^o/τ (d) as a function of oxygen pressure.

To further confirm the validity of ratiometric measurements using R-UiO, the phosphorescence lifetime of R-UiO-1 in HBSS buffer was measured under different pO_2 (Figure 2c). The data were fitted by bi-exponential decay. The amplitude weighted lifetime τ (28.1 μs) in a deoxygenated (0 mmHg) atmosphere steadily decreased as pO_2 increased and reached 7.54 μs in an aerated atmosphere (160 mmHg). The lifetime was fitted according to equation (2) (Figure 2d):

$$\frac{\tau^0}{\tau} = 1 + K_{SV} p_{O_2} \quad (2)$$

where τ^o and τ are weighted lifetimes in the absence and presence of oxygen, respectively. The obtained K_{SV} = 0.017 $mmHg^{-1}$ is similar to the ratiometric measurement result, which indicates negligible static quenching of R-UiO-1.

Next we tested the validity of the ratiometric sensors by CLSM. R-UiO-2 was dispersed in HBSS buffer and subjected to CLSM imaging under different pO_2. Upon excitation with a 514 nm Argon laser, signals in the range of 620-660 nm and 540-580 nm were collected in two separate channels (Figure S17) and analyzed by ImageJ to quantify the intensity ratios, referred as I_P/I_F. Notably, the I_P/I_F - pO_2 curve deviates from that obtained by fluorimetry (Figure 2a), which is reasonable given that the process of collecting photoluminescence on a CLSM is much more complicated than using a fluorimeter. Many factors besides pO_2 such as laser power and dwell time can influence the absolute and relative intensities of phosphorescence/fluorescence.[23] We also noticed that the phosphorescence component was more prominent under CLSM with our instrument settings, so we used R-UiO-2 with a higher RITC loading for CLSM experiments. The I_P/I_F - pO_2 curves obtained by CLSM are highly reproducible with the I_P/I_F ratio gradually decreasing as pO_2 increases, and are fitted with a rational function (Formula S2, SI) which serves as a standard curve for intracellular pO_2 measurements.

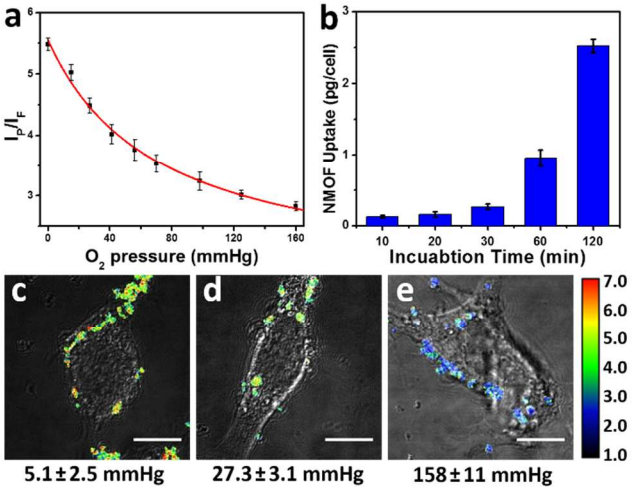

Figure 3. (a) Calibration curve of the phosphorescence/fluorescence intensity of R-UiO-2 on CLSM under different oxygen partial pressures. (b) Time-dependent cellular uptake of R-UiO-2 in CT26 cells determined by ICP-MS. Ratiometric luminescence imaging (λ_{ex} = 514 nm) of CT26 cells after incubation with R-UiO-2 under (c) hypoxia, (d) normoxia, and (e) aerated conditions. Bar: 10 μm.

We chose mouse colon carcinoma CT26 cells with a low background autofluorescence for *in vitro* imaging. The cellular uptake of R-UiO-2 in CT26 cells was first investigated by incubating CT26 cells with 30 μg/mL R-UiO-2 for different times. Cytotoxicity assay indicates that R-UiO is biocompatible (Figure S18). Time-dependent endocytosis was quantified by ICP-MS and shown in Figure 3b. Efficient cellular uptake (~2.5 pg/cell) was observed after a 2 h incubation, which indicates feasibility for intracellular pO_2 measurements.

Finally we used R-UiO-2 to examine cellular O_2 levels. CT26 cells were incubated with R-UiO-2 for 2 h. The culturing media were then exchanged to HBSS buffer with different pO_2 in a sealed chamber, and cells were incubated for another 15 min to ensure efficient oxygen exchange across cell plasma membranes. CLSM settings were identical to those used for the calibration curve. We tested three different pO_2 conditions: 4 mmHg, 32 mmHg, and 160 mmHg, which represent hypoxia, normoxia and aerated conditions, respectively. Different channels of cellular uptake of R-UiO-2 captured by CLSM are shown in Figure S19. The I_P/I_F ratios of R-UiO-2 were shown by pseudocolor images in Figure 3c. The I_P/I_F

values of internalized R-UiO-2 analyzed by ImageJ were 5.29 ± 0.12, 4.45 ± 0.09, and 2.80 ± 0.06, corresponding to 5.1 ± 2.5 mmHg, 27.3 ± 3.1 mmHg, and 158 ± 11 mmHg (see SI for error analysis) respectively according to the calibration curve in Figure 3a. The results matched well with the preset pO_2 in each chamber. These data suggest the broad range and good accuracy of R-UiO as intracellular oxygen sensors.

In conclusion, we have for the first time reported the rational design and synthesis of stable, crystalline, porous, and dual-emissive R-UiO NMOFs for ratiometric sensing of intracellular oxygen in live cells. This study should inspire the design of NMOF sensors for other biologically important analytes by taking advantage of the synthetic tunability, structural versatility, and other unique attributes of NMOFs.

ASSOCIATED CONTENT

Supporting Information

Experimental details for the synthesis and characterization of M-UiO and R-UiO NMOFs, oxygen calibration and fitting, cellular uptake and live cell imaging. This material is available free of charge via the Internet at http://pubs.acs.org.

AUTHOR INFORMATION

Corresponding Author

wenbinlin@uchicago.edu

Author Contributions

†R.X. and Y.W. contributed equally.

Notes

The authors declare no competing financial interests.

ACKNOWLEDGMENT

We thank the NIH (UO1-CA198989 and P30 CA014599) for funding support and Dr. Vytas Bindokas for help with confocal microscopy imaging.

REFERENCES

1. Ikeda, *E. Pathol. Int*. **2005**, *55* , 603-610.
2. Harris, A. L. *Nat. Rev. Cancer* **2002**, *2*, 38-47.
3. Höckel, M.; Schlenger, K.; Aral, B.; Mitze, M.; Schäffer, U.; Vaupel, P. *Cancer Res*. **1996**, *56*, 4509-4515.
4. Gatenby, R. A.; Kessler, H. B.; Rosenblum, J. S.; Coia, L. R.; Moldofsky, P. J.; Hartz, W. H.; Broder, G. *J. Int. J. Radiat. Oncol. Biol. Phys*. **1988**, *14*, 831-838.
5. Hoogsteen, I. J.; Lok, J.; Marres, H. A.; Takes, R. P.; Rijken, P. F.; van der Kogel, A. J.; Kaanders, J. H. *Eur. J. Cancer* **2009**, *45*, 2906-2914.
6. Mees, G.; Dierckx, R.; Vangestel, C.; Van de Wiele, C. *Eur. J. Nucl. Med. Mol. Imaging* **2009**, *36*, 1674-1686.
7. (a) Cooper, R. A.; Carrington, B. M.; Loncaster, J. A.; Todd, S. M.; Davidson, S. E.; Logue, J. P.; Luthra, A. D.; Jones, A. P.; Stratford, I.; Hunter, R. D. *Radiother. Oncol*. **2000**, *57*, 53-59. (b) Padhani, A. R.; Krohn, K. A.; Lewis, J. S.; Alber, M. *Eur. Radiol*. **2007**, *17*, 861-872.
8. (a) Zhang, G.; Palmer, G. M.; Dewhirst, M. W.; Fraser, C. L. *Nat. Mater*. **2009**, *8*, 747-751. (b) Spencer, J. A.; Ferraro, F.; Roussakis, E.; Klein, A.; Wu, J.; Runnels, J. M.; Zaher, W.; Mortensen, L. J.; Alt, C.; Turcotte, R. *Nature*. **2014**, *508*, 269-273. (c) Wu, C.; Bull, B.; Christensen, K.; McNeill, J. *Angew. Chem. Int. Ed*. **2009**, *48*, 2741-2745. (d) Wang, X.-d.; Stolwijk, J. A.; Lang, T.; Sperber, M.; Meier, R. J.; Wegener, J.; Wolfbeis, O. S. *J. Am. Chem. Soc*. **2012**, *134*, 17011-17014. (e) Zhao, Q.; Zhou, X.; Cao, T.; Zhang, K. Y.; Yang, L.; Liu, S.; Liang, H.; Yang, H.; Li, F.; Huang, W. *Chem. Sci*. **2015**, *6*, 1825-1831. (f) Yoshihara, T.; Yamaguchi, Y.; Hosaka, M.; Takeuchi, T.; Tobita, S. *Angew. Chem. Int. Ed*. **2012**, *51*, 4148-4151.
9. Feng, Y.; Cheng, J.; Zhou, L.; Zhou, X.; Xiang, H. *Analyst* **2012**, *137*, 4885-4901.
10. Koo, Y.-E. L.; Cao, Y.; Kopelman, R.; Koo, S. M.; Brasuel, M.; Philbert, M. A. *Anal. Chem*. **2004**, *76*, 2498-2505.
11. Chojnacki, P.; Mistlberger, G.; Klimant, I. *Angew. Chem. Int. Ed*. **2007**, *46*, 8850-8853.
12. Amelia, M.; Lavie-Cambot, A.; McClenaghan, N. D.; Credi, A. *Chem. Commun*. **2011**, *47*, 325-327.
13. (a) Kreno, L. E.; Leong, K.; Farha, O. K.; Allendorf, M.; Van Duyne, R. P.; Hupp, J. T. *Chem. Rev*. **2011**, *112*, 1105-1125. (b) Liu, D.; Lu, K.; Poon, C.; Lin, W. *Inorg. Chem*. **2013**, *53*, 1916-1924. (c) Hu, Z.; Deibert, B. J.; Li, J. *Chem. Soc. Rev*. **2014**, *43*, 5815-5840. (d) Guo, Z.; Song, X.; Lei, H.; Wang, H.; Su, S.; Xu, H.; Qian, G.; Zhang, H.; Chen, B. *Chem. Commun*. **2015**, *51*, 376-379.
14. (a) Yang, W.; Feng, J.; Song, S.; Zhang, H. *ChemPhysChem*. **2012**, *13*, 2734-2738. (b) Suresh, V. M.; Chatterjee, S.; Modak, R.; Tiwari, V.; Patel, A. B.; Kundu, T. K.; Maji, T. K. *J. Phys. Chem. C* **2014**, *118*, 12241-12249. (c) Wu, P.; Wang, J.; He, C.; Zhang, X.; Wang, Y.; Liu, T.; Duan, C. *Adv. Funct. Mater*. **2012**, *22*, 1698-1703.
15. (a) He, C.; Lu, K.; Lin, W. *J. Am. Chem. Soc*. **2014**, *136*, 12253-12256. (b) Taylor, K. M.; Rieter, W. J.; Lin, W. *J. Am. Chem. Soc*. **2008**, *130*, 14358-14359. (c) deKrafft, K. E.; Xie, Z.; Cao, G.; Tran, S.; Ma, L.; Zhou, O. Z.; Lin, W. *Angew. Chem. Int. Ed*. **2009**, *48*, 9901-9904. (d) Hatakeyama, W.; Sanchez, T. J.; Rowe, M. D.; Serkova, N. J.; Liberatore, M. W.; Boyes, S. G. *ACS Appl. Mater. Interfaces* **2011**, *3*, 1502-1510. (e) Foucault-Collet, A.; Gogick, K. A.; White, K. A.; Villette, S.; Pallier, A.; Collet, G.; Kieda, C.; Li, T.; Geib, S. J.; Rosi, N. L. *Proc. Natl. Acad. Sci. U. S. A*. **2013**, *110*, 17199-17204.
16. McKinlay, A. C.; Morris, R. E.; Horcajada, P.; Férey, G.; Gref, R.; Couvreur, P.; Serre, C. *Angew. Chem. Int. Ed*. **2010**, *49*, 6260-6266.
17. Lu, K.; He, C.; Lin, W. *J. Am. Chem. Soc*. **2014**, *136*, 16712-16715.
18. Coppeta, J.; Rogers, C. *Exp. Fluids* **1998**, *25*, 1-15.
19. Manna, K.; Zhang, T.; Greene, F. X.; Lin, W. *J. Am. Chem. Soc*. **2015**, *137*, 2665-2673.
20. (a) Valeur, B.; Berberan-Santos, M. N. Molecular fluorescence: principles and applications. John Wiley & Sons: 2012. (b) Turro, N. J.; Ramamurthy, V.; Scaiano, J. C. Modern molecular photochemistry of organic molecules. Wiley Online Library: 2012.
21. Zhang, G.; Chen, J.; Payne, S. J.; Kooi, S. E.; Demas, J.; Fraser, C. L. *J. Am. Chem. Soc*. **2007**, *129*, 8942-8943.
22. Carreau, A.; Hafny‐Rahbi, B. E.; Matejuk, A.; Grillon, C.; Kieda, C. *J. Cell. Mol. Med*. **2011**, *15*, 1239-1253.
23. Finikova, O. S.; Lebedev, A. Y.; Aprelev, A.; Troxler, T.; Gao, F.; Garnacho, C.; Muro, S.; Hochstrasser, R. M.; Vinogradov, S. A. *ChemPhysChem*. **2008**, *9*, 1673-1679.

TOC Graphic